Enhanced bone regeneration with curcumin incorporated and Sr-substituted biphasic calcium phosphate ceramics: Synthesis, characterisation and biomedical applications

Rojaleen Lenka, Padmaksh Dwibedy, Subhasmita Swain*, Tapash R. Rautray

Biomaterials and Tissue Regeneration Lab., Institute of Technical Education and Research, Siksha 'O' Anusandhan (Deemed to be University), Bhubaneswar – 751030, Odisha, India

Received 29 September 2025; received in revised form 11 November 2025; accepted 25 March 2026

Abstract

Biphasic calcium phosphate (BCP) ceramics are prevalent bone substitutes owing to their potential to accelerate bone development. However, improving the degradation ability and the osteoinductive properties of implantable bone filler BCP ceramics is a technically challenging. The incorporation of strontium (Sr) into BCP can substantially improve the regeneration process, due to the distinct mode of action displayed by Sr, which concurrently enhances osteoblastogenesis while inhibiting osteoclastogenesis. The Sr-incorporated BCP samples were synthesised by aqueous precipitation process and the produced specimen was dip coated with curcumin to enhance the bactericidal impact of the composite. The specimens were characterised physically and biologically to evaluate their phase composition, wettability, biodegradation as well as responses towards biocompatibility, osteogenicity and antibacterial characteristics. According to the XRD data, the hydroxyapatite (HA)-crystals of Sr-BCP were partly converted to the β--tricalcium phosphate (β-TCP) phase after sintering at high temperatures. This came about as the Sr^{2+} partially substituted the Ca^{2+}, and as a result, Ca-deficient HA was synthesised. Antibacterial assay of the synthesized composites demonstrated inhibitory action against S. Aureus bacteria, whereas cell culture using MTT (3-(4,5-dimethylthiazol-2-yl)-2,5-diphenyltetrazolium bromide) assay exhibited enhanced cell proliferation.

***Keywords**: Sr-BCP, osteogenicity, gene expression, bactericidal impact*

I. Introduction

The clinical need for bone transplants is increasing due to diseases including trauma, cancer, infection and arthritis, but only few effective treatment alternatives are available [1–4]. The orthopaedic community consequently demands bone graft materials that have the potential to induce osteogenesis along with antimicrobial properties. Systemic administration of antibiotics has several disadvantages, and usually the problem is that the local effect of the bactericidal dosage is inadequate [5]. Consequently, it is extremely intriguing to investigate the possibilities of biomaterial modification by various components [6]. It would be convenient to synthesise an effective composite bone filler where a natural antimicrobial compounds of plant origin were used for modification that showed resistance to infection or possessed osteogenic characteristics and hence superior properties could be paired with better bioactivity.

Though bone is composed of hydroxyapatite ($Ca_{10}(PO_4)_6(OH)_2$) mineral (HA), organic phase and water [7–13], it would seem normal to integrate a variety of constituents in the bone implant fabrication process to develop a composite bone substitute, permitting increased bioactivity and structural bio-mimicry of the implanted material [14,15]. Certain materials like ceramics, hydrogels and polymers have not been able to replicate the properties of bone accurately when used alone. HA and tricalcium phosphate ($Ca_3(PO_4)_2$) (TCP) are being extensively implemented in tissue engineering to treat and heal bone injuries. Calcium-phosphate-based materials are considered enhanced biomaterials as they carry excellent osteoinductive and osteoconductive properties [16]. In terms of chemical composition, HA possesses similar properties as human enamel, bone and dentine minerals, including a low degradability feature [17], whereas β-TCP shows indications of appropriate degradation. The mixture of HA and β-TCP, referred to as biphasic calcium phosphate (BCP), is commonly regarded as an essential ceramic material

*Corresponding author: tel: +86 13705187680
e-mail: *subhasmitaswain@soa.ac.in*

in bone tissue engineering. HA has extraordinary bioactivity and biocompatibility properties regarding bone cells and tissues, which help to drive osteoinduction [18–23]. It possesses piezoelectric characteristics that allow it to respond to mechanical stress and speed up the repair of significant fractures in broken bones, whereas β-TCP having biocompatible and bioresorbable properties influences angiogenesis. The properties of BCP rely upon the proportion of HA/β-TCP. Generally, the osteoinductive capability of BCP is practically identical to that of HA within the sight of osteoinductive development factors, yet it is higher than both HA and β-TCP without any enhancements. Along with promoting new bone formation, BCP is biocompatible, safe and non-allergenic and at present, BCP has been widely used as a bone substitute or prosthetic coating. With rhombohedral symmetry, BCP has been broadly acknowledged as a preferable biocompatible material over its phase constituents, but regardless of being osteoconductive and osteoinductive in nature, the primary drawback of BCP lies in the poor mechanical properties of its constituent phases [24]. To conquer this disadvantage, the isomorphic replacement of various particles inside HA and β-TCP cross-section structure is possibly the most investigated approach.

The alkali-earth metal strontium (Sr) is known as one of the most vital and osteophilic trace elements in the human body, and has recently become widely employed in bone implant materials because of its superior biological features of suppressing the resorption of bones by encouraging osteogenesis. Strontium ion (Sr^{2+}) has been demonstrated to have dual role in bone maintenance, as it encourages osteoblasts to produce fresh bone matrix and simultaneously inhibits osteoclast activity by lowering the resorption of bones. Though Sr^{2+} shares the same chemical structure and characteristics as Ca^{2+}, according to Cheshmedzhieva *et al*. [25], Sr^{2+} can replace the Ca^{2+} sites in HA giving Sr^{2+} a significant bone-seeking property. According to Wu *et al*. [26], there are two primary routes through which Sr^{2+} enters bone tissue: i) firstly, through the interchange of Sr^{2+} with Ca^{2+}, where the majority of Sr^{2+} enters the crystalline surface of the bone and ii) secondly, a small portion of Sr^{2+} substitutes Ca^{2+} in crystalline hydroxyapatite in bone. Currently, strontium ranelate is a medication used to treat osteoporosis [27] as it can induce osteoblastogenesis as well as suppress osteoclastic activity. Two stable Sr atoms are coupled with ranelic acid, which serves as a carrier, to form strontium ranelate [28]. The results of several studies have demonstrated that a variety of Sr^{2+}-incorporated biomaterials, including Sr^{2+}-incorporated bioactive glasses, coatings, bone cement, etc. can speed up bone growth around the injured bone tissue [29,30].

Staphylococcus Aureus, *Enterococci* and *Pseudomonas Aeruginosa* are the leading causes of infection-related diseases linked to bone implantation [31]. Earlier intervention needs to be taken to avert bacterial infections and the ensuing growth of biofilms during the first few days after surgery because the biofilm infection is frequently resistant to antibiotic treatment due to the application of excessive, persistent antibiotics concentrations, and it could cause systemic toxicity as well as impair *in vivo* bone regenerations [32]. The turmeric rhizome is the source of the antioxidant and antibacterial chemical curcumin (CUR), i.e. 1,7-bis (4-hydroxy-3-methylphenyl)-1,6-heptadiene-3,5-dione. It has potent antibacterial actions on both Gram-negative and Gram-positive strains of bacteria [33,34]. Additionally, curcumin inhibits the growth of biofilms by preventing bacterial quorum sensing signalling transmission. Since curcumin lowers bone turnover, it is potentially helpful for those with moderate osteoporosis to improve graft attachment [35], which may be a further indicator that demonstrates the higher antibacterial properties of curcumin in applications involving bone implants as opposed to those of other antimicrobial substances. According to certain studies, curcumin-doped nano-scaffold acts as a biodegradable and efficient topical drug delivery system that can operate as an antioxidant, speed up the healing process and shield against bacterial infections [36,37].

The objective of the present study is to bring all the benefits of the materials mentioned above together. Therefore, using the wet chemical technique, Sr-doped BCP composites amalgamated with curcumin (Sr-BCP-Cur) were synthesised to accomplish osteoinductivity and antimicrobial characteristics. Gram-positive *S. Aureus* bacteria were used to demonstrate antibacterial efficacy. Finally, its biological characteristics were confirmed *in vitro* using osteoblast-like cells, which were tested for cell cytocompatibility.

II. Experimental

2.1. Fabrication of Sr-doped BCP ceramics

Calcium nitrate tetrahydrate ($Ca(NO_3)_2{\cdot}4H_2O$), strontium nitrate ($Sr(NO_3)_2$), diammonium hydrogen phosphate ($(NH_4)_2HPO_4$) and sodium hydroxide (NaOH) were obtained from Sinopharm Chemical Reagent Co. Ltd. Curcumin (1,7-bis (4-hydroxy-3-methylphenyl)-1,6-heptadiene-3,5-dione), ethanol (Pure, ≥99.5%) and urea were procured from Sigma-Aldrich.

Sr-doped BCP powders with 5 and 10 mol% of Sr (5SrBCP and 10SrBCP, respectively) were synthesised by using an aqueous precipitation procedure, which was previously described by Mohapatra *et al*. [38]. $Ca(NO_3)_2{\cdot}4H_2O$, $Sr(NO_3)_2$ and $(NH_4)_2HPO_4$ solutions

were mixed in gradual succession while the pH was maintained at 11 with the aid of buffer solutions. The solution was aged for 24 h, washed 4–5 times and then filtered to obtain the 5SrBCP and 10SrBCP powders. The resulting powders were then thermally treated at 1000 °C for 2 h. Using a mortar and pestle, the Sr-doped BCP powders were crushed and particles having a size of less than 75 μm were obtained by utilising stainless steel sieves. To generate Sr-BCP composite pellets, the fabricated powders were thoroughly combined with the binding agent urea and ethanol before being compressed through in a hydraulic press at a 20-ton pressure. Finally, the composite pellets were dipped in curcumin solution (1 mg/ml) in ethanol and kept for 24 h for the curcumin to be entirely absorbed by the pellets. The obtained composite samples were denoted as 5SrBCP-CUR and 10SrBCP-CUR.

2.2. Structural characterisation

For qualitative analysis of the crystal structure of the composite specimens, a stepwise X-ray diffractometer having Cu Kα radiation of wavelength 0.154 nm, voltage of 40 kV and current of 20 mA was employed. At a rate of 2 °/min, XRD patterns were recorded in the range of 20° to 80° during the scan.

Microstructure and pore morphology of the prepared composite specimens were investigated by scanning electron microscope (SEM; Zeiss EVO 18, Germany) following Au sputter coating, to obtain high-magnification imaging. The pore size was calculated by selecting arbitrary zone of the specimen attached in SEM.

The water absorption potential of the prepared composites (5SrBCP-CUR and 10SrBCP-CUR) was assessed by immersing a calculated weight of the composites in de-ionised water for a duration of 2 h. Then, the specimens were taken out of the water and dried and their wet weight was calculated. The following formula was used to determine the swelling ratio (*SR*):

$$SR = \frac{m_{wet} - m_{dry}}{m_{dry}} \times 100 \quad (1)$$

where m_{wet} is wet weight and m_{dry} is dry weight.

Wettability of the 5SrBCP-CUR and 10SrBCP-CUR composites was assessed by using simulated body fluid (SBF) and Dulbecco's modified Eagle's medium (DMEM). At a pH of 7.2, the contact angles of the static liquid drops were measured with the help of a predetermined contact angle setup.

2.3. Biodegradation test and MTT assay

Biodegradation of the prepared composites was examined *in vitro* by dipping the samples in SBF solution at 50 mg/ml of solid-to-liquid proportion at 37 °C. To avoid potential pH variations and contamination by microbes, each specimen was stored in a sealed plastic flask. During the experiment, the SBF solution was unchanged. Post-soaking, the specimens were filtered, washed thoroughly using deionised water and left to dry at 40 °C for 4 days before being properly weighed. The percentage of original weight lost was used to compute the weight loss.

Ion release of the 5SrBCP-CUR and 10SrBCP-CUR specimens was determined by dispersing of 500 mg of the obtained composite in 50 ml of SBF. Further, the rise of Ca^{2+} and Sr^{2+} in the SBF was detected using Particle-Induced X-ray emission (PIXE) multi-elemental analysis [39].

Human osteoblast-like MG63 cell lines obtained from NCCS, PUNE, were used and an MTT (3-[4,5-dimethylthiazol-2-yl]-2,5-diphenyltetrazolium bromide) assay was conducted by following the technique used by Swain *et al*. [40]. The produced specimens were cultured at 37 °C in a humidified environment containing 5% CO_2. Dulbecco's modified Eagle's medium (DMEM, Invitrogen, Paisley, UK) was used to culture the cells, that was augmented with 10% foetal bovine serum (FBS, Invitrogen, Paisley, UK), 100 mg/ml streptomycin, and 100 U/ml penicillin. Every other day, the culture media was changed. The MTT assay, which was utilised to quantify cell proliferation by detecting mitochondrial succinate dehydrogenase activity, was again utilised to investigate the cytotoxicity of the produced specimens. The specimens were fixed in the bottom of a 24-well cell culture plate and disinfected for 24 h at room temperature with ethylene oxide (ETO) vapour. Afterwards, 1 ml of the cell suspension was uniformly planted onto each sample. Every two days, the culture medium was replaced with new medium. Following seeding for 1, 3, and 5 days, 100 ml of MTT solution (5 mg/ml) was added to each well and cultivated at 37 °C for four hours to allow the initiation of formazan crystals. After removing cell suspension, 650 ml of dimethyl sulfoxide (DMSO) was added to each well to dissolve the blue formazan crystal and the solution was relocated to 96-well plates. Using an ELISA microplate reader, the absorbance of each well was measured at 570 nm (Bio-Rad).

2.4. Determination of osteogenic gene expression

To determine the level of mRNA gene expression quantitative reverse transcription polymerase chain reaction (q RT-PCR) was conducted following the procedure described by Swain *et al*. [19], in order to evaluate the osteogenic differentiation of MG63 cells on the BCP, 5SrBCP-CUR and 10SrBCP-CUR composite surface. To identify type-1 collagen (COL1A1), Runt-related transcription factor (RUNX2) and osteocalcin (OCN), Bio-Rad MyiQ2 was utilized in conjunction with the Trans Start Top Green qPCR

Super Mix (Transgenic). Before lysing the cells with TRIZOI (Invitrogen) to extract RNA, they were cultured over a period of 1, 3 and 5 days at a density of 4×10^4 per well. The cells from each composite in each group were utilised to get an adequate amount of RNA. By employing the Superscript II First Strand cDNA Synthesis Kit, one milligram of RNA experienced reverse transcription, producing complementary DNA (cDNA) [41].

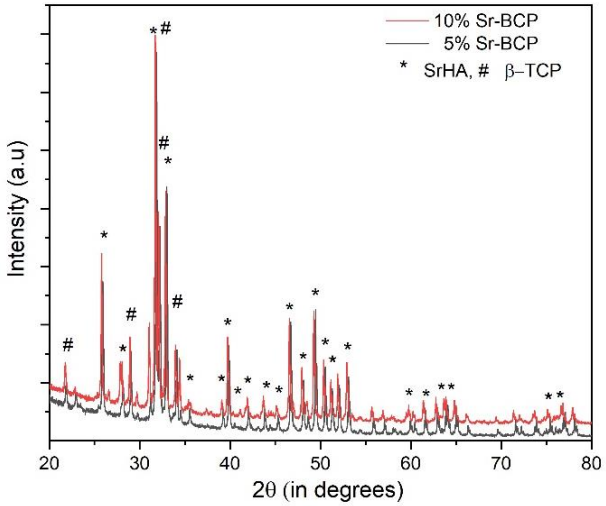

Figure 1. XRD patterns of composite specimens of 5SrBCP and 10SrBCP (* indicates Sr-HA and # indicates β-TCP)

2.5. Bacterial viability test

The antibacterial assessment of the 5SrBCP-CUR and 10SrBCP-CUR bioceramic composites was conducted by using *S. Aureus* bacteria in a similar procedure mentioned by Swain *et al.* [28]. Mueller-Hinton Broth (MHB) medium was used to grow the bacteria. Bacterial viability was measured *in vitro* with the help of the MTT assay. Each measurement yielded an average of three specimens. The specimens were placed in a 24-well culture dish with 1 ml of bacterial cell suspension containing 1×10^6 CFU per ml in each well at 37 °C. The *in vitro* bacteria culture was continued for 10 h, 20 h and 30 h, and the adherent bacteria were tested for viability by mixing 200 µl of bacteria suspension with 200 µl of the MTT solution (5 mg/ml) and incubating for 6 h at 37 °C, resulting in the formation of crystals. At a wavelength of 490 nm, a spectrophotometric microplate reader was used to measure the optical density of the composite solution.

All the experimental outcomes were expressed by using the mean standard deviation. One-way analysis of variance (ANOVA) was employed to compare the variations in the data.

III. Results

3.1. Structure of Sr-doped BCP samples

XRD analysis revealed that the samples contained two phases, i.e. β-TCP and Sr-HA (Fig. 1), with the ratio of 60% β-TCP and 40% HA. The HA and β-TCP standard references were used to identify the phase composition according to the characteristic XRD peaks. According to the XRD results it can be also concluded that the crystallinity of BCP was not changed with Sr-addition. In addition, the peaks of Sr-HA phase are marginally displaced to lower 2θ values as compared to the XRD of the pure HA compound. This could be due to a rise in the lattice parameter and higher *d*-spacing because the ionic radius of Sr^{2+} is slightly larger than that of the Ca^{2+} ion.

Figure 2 shows SEM images of the Sr-doped composites. Both 5SrBCP and 10SrBCP specimens displayed interconnected porous structures which facilitate cell migration and proliferation through diffusion of cells, nutrients and other body fluids. The 5SrBCP and 10SrBCP composites have pore size ranging from 0.457 to 1.02 µm and 0.594 to 1.27 µm, respectively.

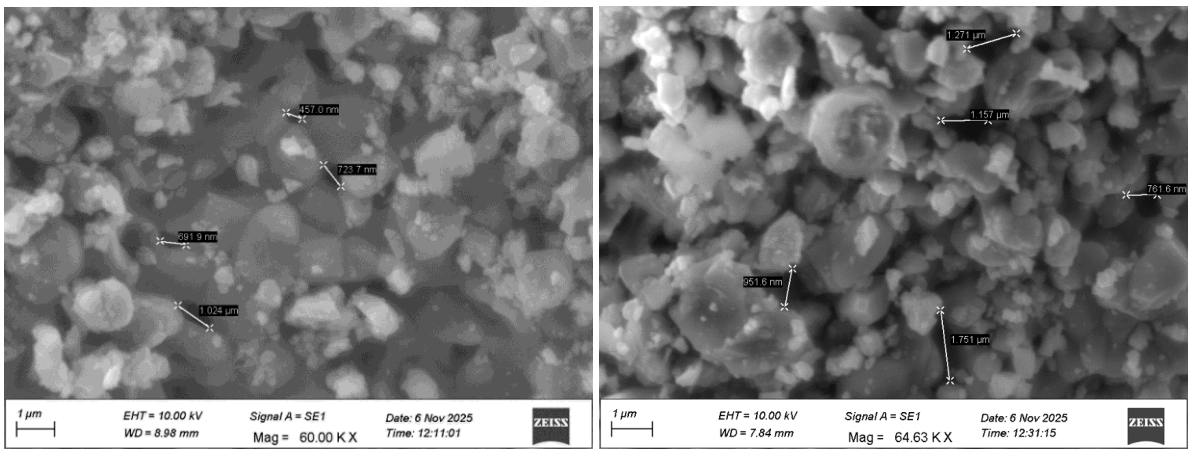

Figure 2. SEM images of 5SrBCP (a) and 10SrBCP (b) composite specimens demonstrating interconnected porous structure

Both 5SrBCP-CUR and 10SrBCP-CUR composites have lower contact angles than the pure BCP sample in both simulated body fluid (SBF) and Dulbecco's modified Eagle's medium (DMEM). The

investigation revealed that cell media (DMEM) contact angle for the 10SrBCP composite was 48° ± 1.9, while contact angle in SBF was 44° ± 1.98. On the other hand, the contact angles in DMEM and SBF with the 5SrBCP composite were measured to be 56° ± 2.22° and 49° ± 2.1°, respectively.

The swelling was the highest in the pure BCP composite, but dropped when the concentration of incorporated ions in the HA lattice grew. As the Sr concentration increased from 5% to 10%, the swelling ratio of the specimens was significantly reduced, as demonstrated in Fig. 3.

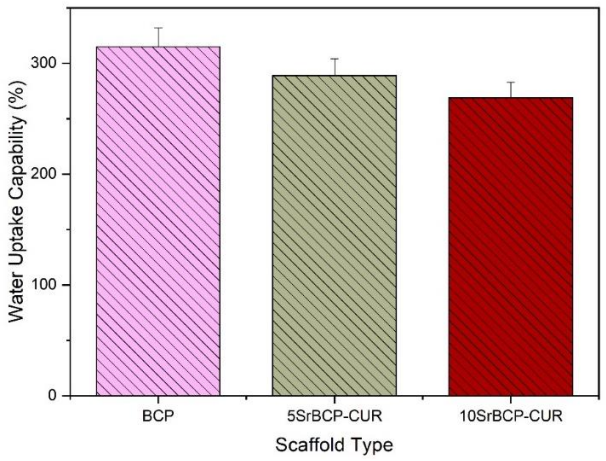

Figure 3. The water uptake capacity of BCP, 5SrBCP-CUR and 10SrBCP-CUR composites

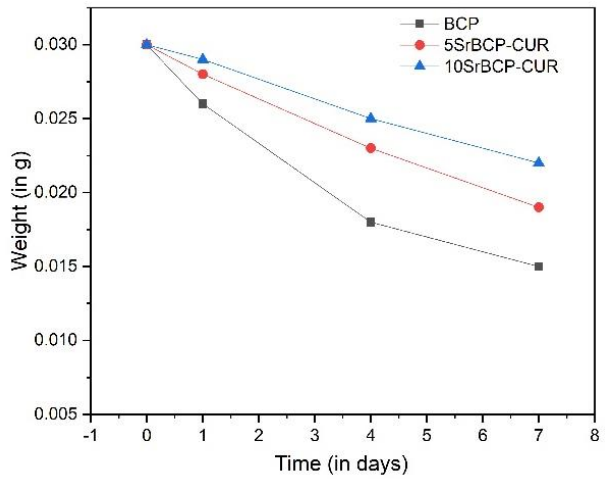

Figure 4. The degradation rate for BCP, 5SrBCP-CUR and 10SrBCP-CUR composite specimens

3.2. Biodegradation and MTT assay

For each specimen, the longer the soaking duration, the faster the specimens degraded. It is concluded that the SrBCP-CUR composites exhibit a lower rate of degradation than the pure BCP composite. After the period of one week, the SrBCP-CUR composites lose less weight than the undoped BCP composite specimen. It can be observed from Fig. 4 that, when the concentration of Sr was increased from 5% to 10%, the degradation rate decreased significantly.

It was also observed that Sr ions were released from the specimens after 12 h and then concentrations ended up at 49 and 57 ppm for the Sr content of 5% and 10%, respectively. The concentration of Sr ion subsequently declined after obtaining the optimum value. The released Sr ions have a significant function in the osteoinductivity characteristic of the SrBCP-CUR composite.

MG63 cell proliferation on the SrBCP-CUR specimens was evaluated by conducting an MTT assay. After being cultured over a period of 1, 3 and 5 days, the cell densities of both specimens were assessed, as shown in Fig. 5. On the 1st, 3rd and 5th day, the cell proliferation rate for the 10SrBCP-CUR was more significant as compared to the 5SrBCP-CUR sample. According to statistical analysis, a considerable variation (p <0.05) was observed in cell density on the surfaces of the SrBCP-CUR (5% and 10%) during all the cultured days.

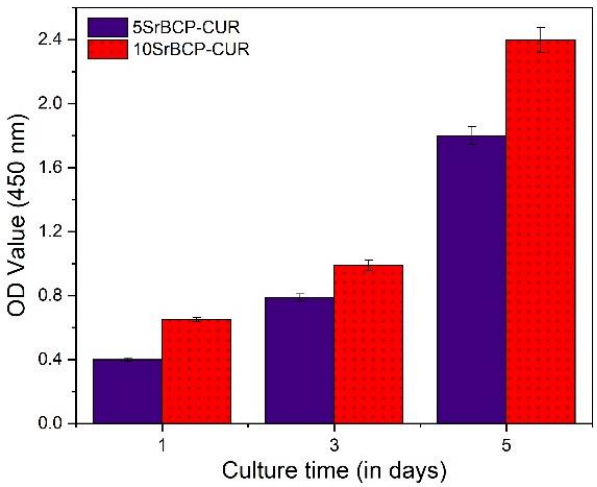

Figure 5. Cell viability on 5SrBCP-CUR and 10SrBCP-CUR composite specimens

3.3. Osteogenic expression

The osteogenic differentiation of MG63 cells on the SrBCP-CUR composites was assessed using the expression level of osteogenic genes involved (Fig. 6). RUNX2, COLIA1 and OCN expressions for MG63 cells on the 10SrBCP-CUR and 5SrBCP-CUR composites were enhanced from 1 to 5 days. In comparison to the 5SrBCP-CUR, the 10SrBCP-CUR composite demonstrated higher gene expression levels (p< 0.05). Table 1 shows the reverse and forward primers for the relevant gene expression.

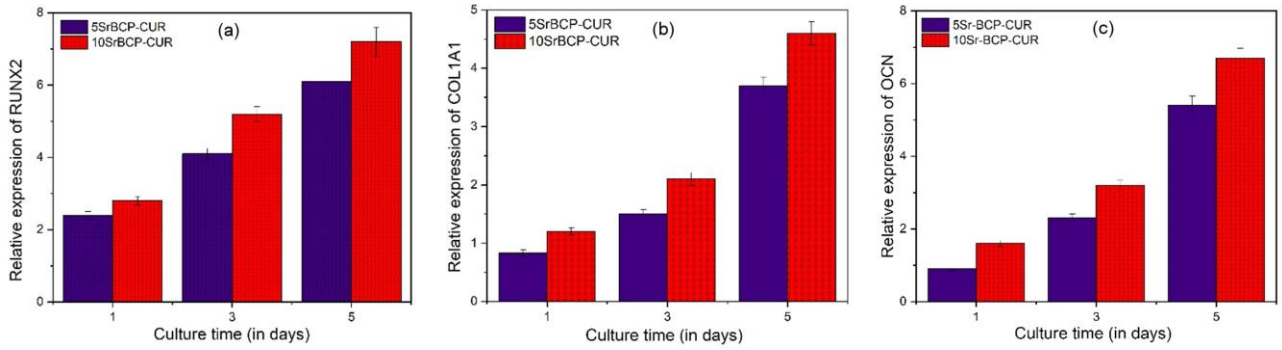

Figure 6. Osteogenic expression of: a) RUNX2, b) COL1A1 and c) OCN on 5SrBCP-CUR and 10SrBCP-CUR composites

Table 1. Primer sequence of gene markers

Gene	Forwarded primer (5′–3′)	Reverse primer (5′-3′)
COL 1A1	GATGATTCCATGTCCCCAAC	GGATTGTTGCAGGTCAGGTT
OCN	TGGTCCCTCAGTCTCATTCC	CGCCTGGGTCTCTTCACTAC
RUNX2	GGATTGGCCCAGGAAATTAT	ACAGTGAGGGGGTGAAACAG

3.4. Bacterial viability

Spectrophotometric microplate reader at wavelength of 490 nm was used to measure the optical density of the composite solution and evaluate the *S. Aureus* bacteria growth. The information was gathered in 10-hour intervals for the 30 h period. In the 10SrBCP-CUR specimens, the number of bacterial cells continues to drop faster over 30 h of culture, as compared to the 5SrBCP-CUR (Fig. 7).

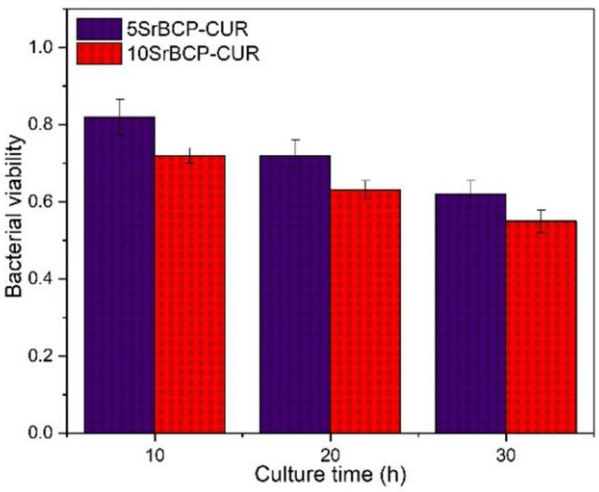

Figure 7. Bacterial viability of *S. Aureus* on 5SrBCP-CUR and 10SrBCP-CUR composites

IV. Discussion

The SrBCP-CUR composites, which were made of well-regulated combinations of non-resorbable Sr-HA as well as resorbable calcium phosphate phase with plant-based chemical curcumin, offers a unique combination of bioactivity, osteogenicity, antibacterial activity as well as structural strength, which is challenging to accomplish in a single-phase material [42].

Osteoblasts and osteocytes are responsible for bone production and mineralisation processes, while osteoclasts are responsible for bone tissue resorption. Sr^{2+} ions are vital during bone regeneration since they activate osteoblasts while simultaneously suppressing osteoclast activity. The Osteoprotegerin (OPG) - RANK ligand (RANKL) system is one of the crucial components in the interaction between osteoclasts and osteoblasts. Pre-osteoblasts and osteoblasts that express RANKL stimulate RANK, which is found on osteoclasts and pre-osteoclasts, causing mature osteoclasts to differentiate and enhance osteoclast survival. OPG, an osteoblast-produced soluble RANKL receptor, prevents RANKL-induced osteoclastogenesis [43]. As a result, the OPG/RANKL ratio is crucial for bone resorption, and it has been shown that in clinical circumstances where bone resorption arises, for instance, in postmenopausal women, the ratio is reduced. It is interesting to note that strontium ranelate upregulates RANKL expression in murine rat calvaria cells while downregulating OPG expression in primary human osteoblast cells *in vitro* [44]. Two different signals are given concurrently when strontium ranelate boosts osteoblasts; its anabolic pathways are triggered in osteoblasts and pre-osteoblasts, while an anti-catabolic message is delivered to osteoclasts and pre-osteoclasts via the rise in the OPG/RANKL ratio.

According to XRD analyses (Fig. 1) the SrBCP specimens do not exhibit presence of any impurity phase. Sr substitution in HA impacts physical properties like lattice parameters, crystal domain size, crystal structure, solubility and thermal stability. The Sr^{2+} replaces Ca^{2+} within the HA structure of SrBCP, resulting in a Ca-deficient HA phase that exhibits

reduced stability at elevated temperatures and is susceptible to transitioning into the substantially more stable β-TCP phase. The transformation induced by strontium modifies the characteristics of the composite, promoting it as a potential bone graft substitute owing to its improved bioactivity and resorbability in comparison to pure HA.

Swain *et al*. [45] showed that Sr has a dual bone production and resorption mechanism by boosting osteoblast activity and lowering osteoclast activity. Compared to the undoped BCP, the crystallinity demonstrated by HA and β-TCP for SrBCP-CUR was elevated. Moreover, 5% Sr-doped BCP powder had higher β-TCP peak intensity with lower HA peak intensity and thus the highest level of β-TCP was found at this Sr concentration. The solubility limit of Sr in HA could explain this phenomenon. The production of β-TCP as a secondary phase was most likely triggered by Sr doping below 5% in HA, while the surplus of Sr concentration beyond 5% stabilised the HA phase, preventing the development of a secondary phase. Furthermore, the reduction in β-TCP amount led to an upsurge in peak intensity of HA at higher concentrations of Sr. The peak intensity of HA was adjusted by elevating the β-TCP peak by Sr doping and the reverse was true. The β-TCP peak was found to be boosted by adding 5% of Sr when it replaced Ca ion in the β-TCP phase. The phase breakdown can be delineated by following a 1000 °C thermal treatment, Sr ions to the β-TCP structure settle down. In previous studies, Sr was observed to partially fill Ca^{2+} sites in the β-TCP structure.

In comparison to the pure BCP, 5SrBCP-CUR and 10SrBCP-CUR have higher contact angle due to their lower hydrophilicity. The wettability of biomaterials influences cell proliferation, adhesion and differentiation on the surface of biomaterials. Furthermore, when the Sr concentration in the composite increased, contact angles were lowered. In tissue engineering, the swelling ability of a composite specimen significantly impacts cell activities such as adhesion, growth and proliferation [46]. It is advantageous for cell development on these composites that all the synthesised specimens have water absorption capacities greater than 100%. The modification in the microenvironment caused by the deteriorated composite specimen at the implant site significantly impacts new bone growth. All the synthesised composite specimens were very slow to degrade and showed a constant rate of deterioration.

As the significant components of bioapatite, Ca and P play critical roles in bone production and resorption. *In vitro,* Ca has been shown to impact osteoblast cells. Low Ca^{2+} concentrations (2–4 mmol) as well as medium Ca^{2+} concentrations (6–8 mmol) are appropriate for osteoblastic differentiation, proliferation and extracellular matrix remineralisation [47]. However, Sr appears to be involved in osteoblast differentiation and proliferation in a supportive capacity too. Sr^{2+} ion, for example, increases the expression of matrix Gla protein, a bone formation regulator in osteoblast cells. The specimen was immersed in SBF at a temperature of 37 °C and concentrations of ions were quantified using PIXE at different time periods to evaluate the ion release capabilities of the SrBCP-CUR composites. In addition to ion release, the phase abundance of β-TCP and Sr-HA regulates cell viability and functionality. The solubility and, thus, Ca^{2+} ion release increase as the amount of β-TCP phase increases, which has an impact on cell survival. On day 5, however, the cell survival rate of the doped SrBCP-CUR composites (5% and 10%) was higher than that of the pure BCP composite. This showed that the presence of Sr caused the growth of MG63 cells [48].

COL1A1, OCN and RUNX2 were used to determine the expression levels of MG63 osteoblast-specific genes using RT-PCR. During the proliferative and matrix maturation phases, COL1A1 is a unique early-stage marker of osteoblast differentiation. On days 3 and 5, the collagen gene expression of MG63 cells was much higher on the doped 10SrBCP-CUR composite, implying that a higher concentration of Sr triggered the cells to proliferate and differentiate. RUNX2 regulates OCN, which is a target gene for the protein. The maturity of osteoblasts was evidenced by an increase in OCN gene expression [49,50]. OCN is an osteogenic differentiation late-stage marker.

The antibacterial properties of the SrBCP-CUR composites were examined using *S. aureus* bacteria, the majority of which were linked to human diseases. Compared to the 5SrBCP-CUR composite, the 10SrBCP-CUR demonstrated improved antibacterial function. The ability of the Sr^{2+} ion along with curcumin to inhibit bacterial growth leads to the disruption of the bacterial cell membrane and other cell components. This may be a reasonable theory for such antimicrobial behaviour.

V. Conclusions

Sr-doped biphasic calcium phosphate (BCP) powders (with 5 and 10 mol% of Sr), synthesised by aqueous precipitation, were calcined at 1000 °C and in the form of pellets dip coated with curcumin. It was inferred that the 10SrBCP-CUR composite specimen induced a higher number of MG63 cells than its counterpart with 5% Sr, which may be ascribed to the higher osteogenicity of Sr. It was also found that both composite specimens suppressed bacterial activities in the presence of curcumin. The obtained results confirmed that the 10SrBCP-CUR composite is a more suitable material for tissue engineering applications than the undoped BCP and 5SrBCP-CUR composite.

References

1. T.R. Rautray, R. Narayanan, K.H. Kim, "Ion implantation of titanium based biomaterials", *Prog. Mater. Sci.*, **56** [8] (2011) 1137–1177.
2. S. Swain, T.R Rautray, "Effect of surface roughness on titanium medical implants". pp. 55–80 in *Proceedings of Nanostructured Materials and their Applications*. Eds. B.P. Swain, Materials Horizons: From Nature to Nanomaterials, Springer, Singapore, 2021.
3. Jr Wallace, J. Richard, B.A. Brown, G.O. Onyi, "Skin, soft tissue, and bone infections due to Mycobacterium chelonae chelonae: importance of prior corticosteroid therapy, frequency of disseminated infections, and resistance to oral antimicrobials other than clarithromycin", *J. Infect. Dis*., **166** [2] (1992) 405–412.
4. S. Swain, S. Kumari, P. Swain, T. Rautray, "Polarised strontium hydroxyapatite–xanthan gum composite exhibits osteogenicity in vitro", *Mater. Today Proc.*, **62** (2022) 6143–6147.
5. S.L. Henry, K.P. Galloway, "Local antibacterial therapy for the management of orthopaedic infections: pharmacokinetic considerations", *Clin. Pharmacokinet.*, **29** [1] (1995) 36–45.
6. S. Swain, R.N. Padhy, T.R. Rautray, "Polarized piezoelectric bioceramic composites exhibit antibacterial activity", *J. Mater. Sci. Mater. Med.*, **239** (2020) 122002.
7. S. Das, S. Swain, T.R. Rautray, "Incorporation of hydroxyapatite and cerium oxide nanoparticle scaffold as an antibacterial filler matrix for biomedical applications", *Int. J. Artif. Organs.*, **47** [5] (2024) 356–361.
8. S. Swain, R. Lenka, T.R. Rautray, "Synthetic strategy for the production of electrically polarized polyvinylidene fluoride-trifluoroethylene. Co-polymer osseo-functionalized with hydroxyapatite scaffold", *J. Biomed. Mater. Res. A*, **112** [10] (2024) 1675–1687.
9. S. Swain, A.K. Dubey, T.R. Rautray, "Unveiling the biomaterial facet of polarized piezoelectric sodium potassium niobate: A comprehensive study", *Mater. Sci. Eng. R*, **167** (2026) 101111.
10. S. Mishra, S. Swain, T.R Rautray, "Preparation of eggshell derived HA-BT composite for biomedical applications", *Integr. Ferroelectr.*, **240** [1] (2024) 163–174.
11. M. Pradhan, S. Swain, T.R. Rautray, "Electrically polarized hydroxyapatite with Sr containing barium titanate incorporated with mangiferin for enhanced osteogenic and antibacterial activity", *Ferroelectrics*, **618** [4] (2024) 1157–1169.
12. T.R. Rautray, K.H. Kim, "Nanoelectrochemical coatings on titanium for bioimplant applications", *Mater. Technol.*, **25** [3-4] (2010) 143–148.
13. S. Swain, T.R. Rautray, R Narayanan, "Sr, Mg, and Co substituted hydroxyapatite coating on TiO_2 nanotubes formed by electrochemical methods", *Adv. Sci. Lett.*, **22** [2] (2016) 482–487.
14. G. Tripathi, B. Basu, "A porous hydroxyapatite scaffold for bone tissue engineering: Physico-mechanical and biological evaluations", *Ceram Int.*, **38** [1] (2012) 341–349.
15. H. Shi, Z. Zhou, W. Li, Y. Fan, Z. Li, J. Wei, "Hydroxyapatite based materials for bone tissue engineering: A brief and comprehensive introduction." *Crystals*, **11** [2] (2021) 149.
16. J. Jeong, J.H. Kim, J.H. Shim, N.S. Hwang, C.Y. Heo, "Bioactive calcium phosphate materials and applications in bone regeneration", *Biomater. Res.*, **23** [1] (2019) 4.
17. D.R. Behera, P. Nayak., T.R. Rautray, "Phosphatidylethanolamine impregnated Zn-HA coated on titanium for enhanced bone growth with antibacterial properties", *J. King Saud Univ. Sci.*, **32** [1], (2020) 848–852.
18. S. Mofakhami, E. Salahinejad, "Biphasic calcium phosphate microspheres in biomedical applications", *J. Control. Release*, **338** (2021) 527–536.
19. S. Swain, S. Mishra, A. Patra, R. Praharaj, T. Rautray, "Dual action of polarised zinc hydroxyapatite-guar gum composite as a next generation bone filler material", *Mater. Today: Proc.*, **62** (2022) 6125–6130.
20. T.R. Rautray, V. Vijayan, S. Panigrahi, "Synthesis of hydroxyapatite at low temperature", *Ind. J. Phys.*, **81** (2007), 95–98.
21. S. Swain, R.N. Padhy, T.R. Rautray, "Electrically stimulated hydroxyapatite–barium titanate composites demonstrate immunocompatibility in vitro", *J. Korean Ceram. Soc.*, **57** [5] (2020) 495–502.
22. S. Swain, R.N. Padhy, T.R. Rautray, "Polarized piezoelectric bioceramic composites exhibit antibacterial activity", *Mater. Chem. Phys.*, **239** (2020) 122002.
23. T.R. Rautray, K.H. Kim, "Synthesis of silver incorporated hydroxyapatite under magnetic field", *Key Eng. Mater.* **493** (2012) 181–185.
24. I. Zarkesh, M.H. Ghanian, M. Azami, F. Bagheri, H. Baharvand, J. Mohammadi, M.B. Eslaminejad, "Facile synthesis of biphasic calcium phosphate microspheres with engineered surface topography for controlled delivery of drugs and proteins", *Colloids Surf. B*, **157** (2017) 223–232.
25. D. Cheshmedzhieva, S. Ilieva, E.A. Permyakov, S.E. Permyakov, T. Dudev, "Ca^{2+}/Sr^{2+} selectivity in calcium-sensing receptor (CaSR): implications for strontium's anti-osteoporosis effect", *Biomolecules*, **11** [11] (2021) 1576.
26. Y. Wu, S.M. Adeeb, M.J. Duke, D. Munoz-Paniagua, M.R, Doschak, "Compositional and material properties of rat bone after bisphosphonate and/or strontium ranelate drug treatment", *J. Pharm. Pharm Sci*., **16** [1] (2013) 52–64.
27. R. Praharaj, S. Mishra, T.R. Rautray, "The structural and bioactive behaviour of strontium-doped titanium dioxide nanorods", *J. Korean Ceram. Soc.*, **57** [3] (2020) 271–280.
28. S. Swain, C. Bowen, T. Rautray, "Dual response of osteoblast activity and antibacterial properties of polarized strontium substituted hydroxyapatite—Barium strontium titanate composites with controlled strontium substitution", *J. Biomed. Mater. Res.*, **109** [10] (2021), 2027–2035.
29. R.D. Prabha, B.P. Nair, N. Ditzel, J. Kjems, P.D. Nair, M. Kassem, "Strontium functionalized scaffold for bone tissue engineering", *Mater. Sci. Eng. C.*, **94** (2019) 509–515.
30. S. Kargozar, M. Montazerian, E. Fiume, F. Baino, "Multiple and promising applications of strontium (Sr)-containing bioactive glasses in bone tissue engineering", *Front. Bioeng. Biotechnol*., **7** (2019) 161.

31. E. Seebach, K.F. Kubatzky, "Chronic implant-related bone infections: Can immune modulation be a therapeutic strategy?", *Front. Immunol.*, **10** (2019) 1724.
32. C.R. Rathbone, J.D. Cross, K.V. Brown, C.K. Murray, J.C. Wenke, "Effect of various concentrations of antibiotics on osteogenic cell viability and activity", *J. Orthop. Res.*, **29** [7] (2011) 1070–1074.
33. D. Praditya, L. Kirchhoff, J. Brüning, H. Rachmawati, J. Steinmann, E. Steinmann, "Anti-infective properties of the golden spice curcumin", *Front. Microbiol.*, **10** (2019) 912.
34. S.Y. Teow, K. Liew, S.A. Ali, A.S.B. Khoo, S.C. Peh, "Antibacterial action of curcumin against Staphylococcus aureus: a brief review", *J. Trop. Med.*, **2016** [1] (2016) 2853045.
35. M. Hatefi, M.R.H. Ahmadi, A. Rahmani, M.M. Dastjerdi, K. Asadollahi, "Effects of curcumin on bone loss and biochemical markers of bone turnover in patients with spinal cord injury", *World Neurosurg.*, 114 (2018) e785–e791.
36. P. Tyagi, M. Singh, H. Kumari, A. Kumari, K. Mukhopadhyay, "Bactericidal activity of curcumin I is associated with damaging of bacterial membrane", *PloS one*, **10** [3] (2015) e0121313.
37. K. Khezri, S. Maleki Dizaj, Y. Rahbar Saadat, S. Sharifi, Shahi, E. Ahmadian, A. Eftekhari, E. Dalir Abdolahinia, F. Lotfipour, "Osteogenic differentiation of mesenchymal stem cells via curcumin-containing nanoscaffolds", *Stem Cells Int.*, **2021** [1] (2021) 1520052.
38. B. Mohapatra, T.R. Rautray, "Strontium-substituted biphasic calcium phosphate scaffold for orthopedic applications", *J. Korean Ceram. Soc.*, **57** [4] (2020) 392–400.
39. S. Swain, T.R. Rautray, "Estimation of trace elements, antioxidants, and antibacterial agents of regularly consumed Indian medicinal plants", *Biol. Trace Elem. Res.*, **199** [3] (2021) 1185–1193.
40. S. Swain, R.D.K. Misra, C.K. You, T.R. Rautray, "TiO_2 nanotubes synthesised on Ti-6Al-4V ELI exhibits enhanced osteogenic activity: A potential next-generation material to be used as medical implants", *Mater. Technol.*, **36** [7] (2021) 393–399.
41. S. Swain, J.L. Ong, R. Narayanan, T.R. Rautray, "Ti-9Mn β-type alloy exhibits better osteogenicity than Ti-15Mn alloy in vitro", *J. Biomed. Mater. Res. B*, **109** [12] (2021) 2154–2161.
42. K. Xue, P.H. Tan, Z.H. Zhao, L.Y. Cui, M.B. Kannan, S.Q. Li, C.B. Liu, Y.H., Zou, F. Zhang, Z.Y. Chen, R.C. Zeng, "In vitro degradation and multi-antibacterial mechanisms of β-cyclodextrin@curcumin embodied $Mg(OH)_2$/MAO coating on AZ31 magnesium alloy", *J. Mater. Sci. Technol.*, **132** (2023) 179–192.
43. T.C. Brennan, M.S. Rybchyn, W. Green, S. Atwa, A.D. Conigrave, R.S. Mason, "Osteoblasts play key roles in the mechanisms of action of strontium ranelate", *Brit. J. Pharmacol.*, **157** [7] (2009) 1291–1300.
44. E. Bonnelye, A. Chabadel, F. Saltel, P. Jurdic, "Dual effect of strontium ranelate: stimulation of osteoblast differentiation and inhibition of osteoclast formation and resorption in vitro", *Bone*, **42** [1] (2008) 129–138.
45. S. Swain, R.D.K. Misra, T.R. Rautray, "Ceragenin-CSA13 loaded high strength coatings of nano-and micro-SrHA implanted N-Carboxymethyl chitosan Polyetheretherketone by low temperature high speed collision approach: In vitro pro-osteogenicity and bactericidal activity against MRSA", *Mater. Chem. Phys.*, **309** (2023) 128367.
46. J. You, Y. Zhang, Y. Zhou, "Strontium functionalized in biomaterials for bone tissue engineering: A prominent role in osteoimmunomodulation", *Front. Bioeng. Biotechnol.*, **10** (2022) 928799.
47. S. Swain, J.R. Koduru, T.R. Rautray, "Mangiferin-enriched Mn–hydroxyapatite coupled with β-TCP scaffolds simultaneously exhibit osteogenicity and anti-bacterial efficacy", *Materials*, **16** [6] (2023) 2206.
48. O. Fromigué, E. Haÿ, A. Barbara, P.J. Marie, "Essential role of nuclear factor of activated T cells (NFAT)-mediated Wnt signaling in osteoblast differentiation induced by strontium ranelate", *J. Biol. Chem.*, **285** [33] (2010) 25251–25258.
49. R. Lenka, S. Swain, T.R. Rautray, "Electrically polarized La-substituted HA-BST composite shows enhanced osteoblast activities and inhibits S. Aureus bacteria", *Biomed. Mater. Devices*, **4** (2025) 531−524.
50. I. Priyadarshini, S Swain, J.R. Koduru, T.R. Rautray, "Electrically polarized with aferin a and alginate-incorporated biphasic calcium phosphate microspheres exhibit osteogenicity and antibacterial activity in vitro", *Molecules*, **28** [1] (2022) 86.